REENTRY SURVIVABILITY ANALYSIS OF THE HUBBLE SPACE TELESCOPE (HST)

R. Smith[(1)], K. Bledsoe[(2)], J. Dobarco-Otero[(1)], W. Rochelle[(1)], N. Johnson[(3)], A. Pergosky[(4)], M. Weiss[(5)]

[(1)]ESC Group/Jacobs Sverdrup, PO Box 58447, Mail Code 5WB, Houston, TX, 77258, U SA, Email: Ries.Smith@escg.jacobs.com
[(2)]Georgia Tech University, Atlanta, GA, USA, Email: gte425z@mail.gatech.edu
[(3)]Orbital Debris Program Office, NASA JSC, Houston, TX, USA, Email: nicholas.l.johnson@nasa.gov
[(4)]Lockheed Martin, NASA GSFC, Greenbelt, MD, USA, Email: apergosky@hst.nasa.gov
[(5)]Hubble Space Telescope Program, NASA GSFC, Greenbelt, MD, USA, Email: michael.l.weiss@nasa.gov

ABSTRACT/RESUME

An analysis of reentry survivability and population risk of the Hubble Space Telescope (HST) entering from orbital decay was performed using the Object Reentry Survival Analysis Tool (ORSAT). The objective was to investigate the reentry, breakup, demise, and ground impact of all objects with known properties. The analysis assumed an uncontrolled reentry from an altitude of 122 km to a breakup altitude of 78 km. Over 600 different objects from the satellite were modeled, comprising 75% of the entire spacecraft mass. A total of 2055 kg of mass is predicted by the analysis to survive reentry and produce an effective debris casualty area of 146 m^2. The resulting calculated risk is 1:250, corresponding to a reentry in the year 2021. The risk has been scaled to account for the unmodeled mass.

1. INTRODUCTION

The Hubble Space Telescope (HST) was delivered to an orbit altitude of 569 km and inclination of 28.5° by the shuttle Discovery during flight STS-31 in April of 1990 (STScI, 2004). The HST is part of the National Aeronautics and Space Administration (NASA) Origins mission to learn more about the history and origin of the universe. The HST has been serviced four times since launch. Without further servicing, the telescope is currently expected to cease functioning in approximately 2008. The HST Deputy Program Manager / Technical of NASA Goddard Space Flight Center (GSFC) requested a reentry survival analysis to calculate the risk to human population for the scenario that the HST orbit would be allowed to decay naturally. The objective of this paper is to describe the method and results of the HST orbital decay reentry survivability analysis using the NASA Johnson Space Center (JSC) Object Reentry Survival Analysis Tool (ORSAT) version 5.8 (Rochelle, 1999a and Dobarco-Otero, 2002) on the spacecraft. The detailed results of this study have been documented (Smith, 2004).

2. DESCRIPTION OF SPACECRAFT

The HST, which can be seen in Fig. 1 (Kerrod, 2003), is cylindrical in shape with a diameter of 4.6 m, a length of 13 m, and the current weight is 11793 kg. Approximately 75% of that mass was modeled for the purposes of this analysis. Another 16% of the mass was accounted for but lacking enough description to model properly. The spacecraft is roughly composed of three general systems: the spacecraft systems, the instruments, and the optics (STScI, 2004).

3. METHOD OF ANALYSIS

ORSAT, which was developed by NASA Johnson Space Center (JSC) and Lockheed Martin Space Operations (LMSO) (Rochelle et al., 1999a), has been used to analyze reentry survivability of 20 spacecraft and launch vehicle upper stages in the last 10 years. The code was validated with barium fuel rod reentry data (Erickson, 1964) and with results of objects recovered after entry (Rochelle et al., 1999b). ORSAT was used in making benchmark calculations (Rochelle et al., 1999c) of reentering hollow spheres, which compared well with those of the European Spacecraft Atmospheric Reentry and Aerothermal Break-up (SCARAB) code (Fritsche et al., 2000). Six general sections of code exist within ORSAT: trajectory, atmosphere, aerodynamics, aerothermodynamics, thermal/ablation, and risk.

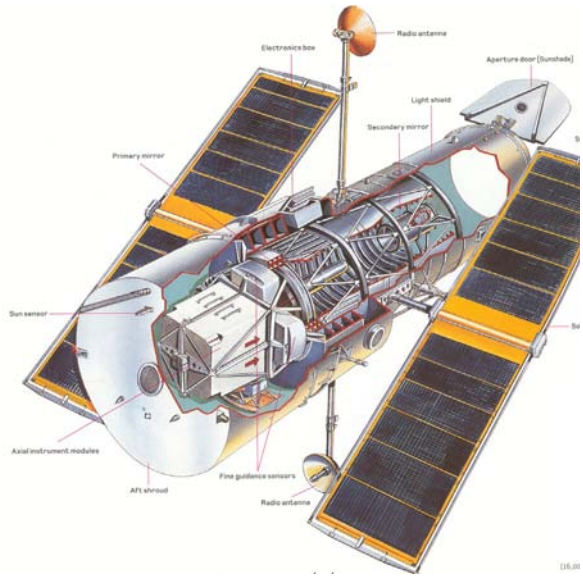

Figure 1. Cut-away View Drawing of the Hubble Space Telescope.

3.1. Trajectory

A 3-Degree-of-Freedom (3-DOF) trajectory is propagated in ORSAT by integrating relative equations of motion for the time rate of change of altitude, relative velocity, relative flight path angle, and longitude. A 4th order Runge-Kutta numerical scheme is used to solve these trajectory equations in ORSAT. An orbital decay reentry was assumed for the HST analysis. This option requires that the initial altitude, relative velocity, relative flight path angle, and inclination angle be input for trajectory calculations. There is also an option for targeted entries that requires the height of apogee and perigee instead of the velocity and flight path angle. For both options the latitude and longitude can be entered. But in the case of an orbital decay, where the time and place of entry is unknown, the latitude and longitude were each set to zero. After the 78 km break-up of the spacecraft each fragment must be given initial trajectory conditions equal to the final conditions of the spacecraft at break-up.

3.2. Atmosphere

The atmosphere model used for the HST reentry analysis was the 1976 US Standard Atmosphere Model. This model is a steady-state (year round) model of the Earth's atmosphere at latitude 45° N during moderate solar activity. It compares well with a higher-fidelity atmosphere model in the code, and has a shorter run-time.

3.3. Aerodynamics

The ballistic coefficient, computed as the mass per area of the object divided by the drag coefficient (m/C_DA), is an important factor in trajectory equations for time rate of change of velocity. The drag coefficient (C_D) is determined based on the type of object (sphere, cylinder, box, or flat plate), the flow regime (continuum, transitional, or free-molecular), the orientation (spinning, tumbling, etc.), and the Mach number. The mass per area (m/A) can change as the object begins to ablate and a layer of material is removed.

3.4. Aerothermal

Convective heating rates for objects in ORSAT are computed based on object geometry, Stanton No., and Knudsen No. The stagnation point cold wall heating rate to a sphere in continuum flow is obtained using the Detra, Kemp, and Riddell method (Detra, 1957). ORSAT also has the capability to consider real gas effects on aeroheating using a Fay and Riddell method (Fay, 1958), but was not used for this analysis. To obtain average heating rates about the object, the sphere stagnation point heating rates are multiplied by factors that account for the average heating over the surface due to rotation and geometric dimensions of the object shape.

The net heating rate is computed as the sum of the hot wall convective heating rate, the oxidation heating rate, and the gas cap radiative heating rate (negligible for orbital or suborbital entry), minus the reradiative heating rate. The oxidation heating rate is based on the heat of oxidation of the material and an oxidation efficiency. The reradiation heat rate is based on the time-varying wall temperature raised to the fourth power and the surface emissivity. The net heating rate is integrated over time and multiplied by the object surface area to predict the absorbed heat on the object as used in the thermal analysis.

3.5. Thermal / Ablation

A 1-D heat conduction model was used in all cases, with the exception of many flat plates that were too thin to be modeled accurately with many nodes. The conduction model uses a forward-time-central-space finite-difference solution to determine the temperature response. The number of nodes used in the objects varied depending on the number of material layers; however, in general either 5 nodes or 10 nodes were used for most objects. After the surface reaches the melting temperature and the net heat absorbed into the outer layer exceeds the material heat of ablation for that layer, then the layer is removed. The boundary conditions are then applied to the new outer layer and the simulation continues until no layers remain or the object reaches the surface of the earth. The simpler lumped mass model computes the object temperature as shown in Eq. 1.

$$T_{surface} = T_{initial} + \frac{H_{absorbed}}{mC_p} \tag{1}$$

After the melting temperature is reached, the surface temperature remains constant until the absorbed heat reaches the heat of ablation. For both models the object is considered to completely demise when the total absorbed heat exceeds the calculated heat of ablation, which is defined in Eq. 2.

$$H_{ablation} = m\left[h_f + \int_{Tinitial}^{Tmelt} C_p dT\right] \tag{2}$$

3.6. Risk

Objects that survive reentry will impact the Earth and contribute to the risk for the Earth's population. The total debris casualty area is the sum of individual debris casualty areas of the surviving objects. Any object that impacts the ground with a kinetic energy below an established threshold (15 J) (Cole, 1996) can be ignored for the purposes of calculating risk. Individual debris casualty area is computed as shown in Eq. 3, where A_{ref}

is the reference area of the object at impact and the number 0.6 represents the square root of the average cross sectional area of a standing individual.

$$DCA = \left(\sqrt{A_{ref}} + 0.6\right)^2 \qquad (3)$$

The expected probability of a casualty can be computed by multiplying the total debris casualty area times the product of the probability of impact in a region times the population density of that region. The region impact probability and population density are averaged based on orbit inclination band (Dobarco-Otero, 2002).

3.7. Assumptions

The trajectory simulation of the entire HST began at an assumed entry interface altitude of 122 km from a 28.5° inclination orbit. The satellite was assumed to break-up into smaller fragments when it reached an altitude of 78 km. This point is the approximate altitude at which a majority of satellites break up according to observations by Aerospace Corp. (Refling, 1992). After the break-up altitude, most of the individual components split from the parent spacecraft and are assumed to be free flying. Further fragmentation may occur and subcomponents will be released if an outer shell or housing has demised. For all HST component surfaces, oxidation heating was assumed with an efficiency (τ) of 0.5 and the initial temperature was assumed to be 300 K when first exposed to the atmosphere.

4. RESULTS

This section describes the results of the orbital decay reentry analysis of HST. Sample plots of trajectory and aerothermal parameters are included to help illustrate the ORSAT results. These plots include both demising and surviving components. The demising objects include the Magnetic Torquer and one of the Near Infrared Camera and Multi-Object Spectrometer (NICMOS) Main Electronic Boxes along with the NICMOS Housing, which is the parent to the NICMOS Main Electronic Boxes. When the NICMOS Housing demises, then the Main Electronic Box is exposed to reentry heating and descends alone. The surviving objects include the Primary Mirror and the Reaction Wheel Assembly (RWA) Flywheel, along with the RWA Housing, which is the parent to the Flywheel. The "parent-child" relation can be seen here again. When the Housing demises, the Flywheel will be exposed. The objects chosen as samples represent all three major systems of the spacecraft.

4.1. Trajectory

The ballistic coefficient is one of the most important factors in reentry analysis. This coefficient dominates the trajectory and determines the velocity profile. The velocity in turn affects the heating rate. Fig. 2 displays the ballistic coefficient versus time during the descent of the sample HST objects. In ORSAT simulations, there are only three ways the ballistic coefficient changes and all three ways are shown in Fig. 2. The initial increase in ballistic coefficient of the Magnetic Torquer is due to flow regime transition. The stepwise decreases in the demising objects show change in mass per area due to ablation. And finally, the surviving objects show changes at later times when they pass through supersonic into subsonic velocities.

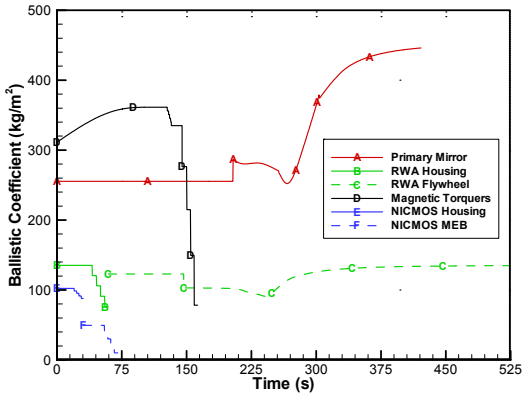

Figure 2. Ballistic coefficient for sample objects.

Fig. 3 shows the altitude plotted against the downrange for all the sample objects. The lines are nearly indistinguishable soon after the breakup, where they are released at the same time and place. However, the two sample parent objects demise and release their corresponding fragments. The trajectories of the objects begin to stray from each other as the effects of the different ballistic coefficients begin to show.

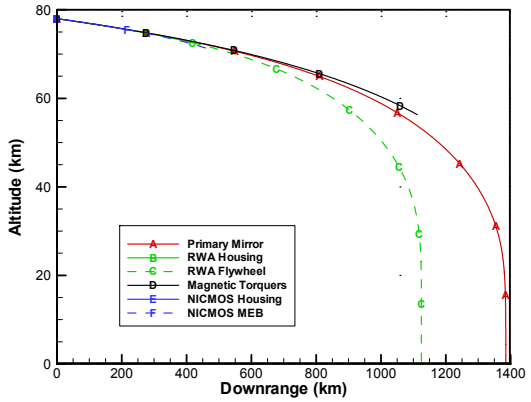

Figure 3. Altitude vs. downrange for sample objects.

The velocity versus downrange for the sample objects are shown in Fig. 4. The magnitude of these velocities has a direct impact on the heating rate to the object. The rate at which these velocities drop is affected by the ballistic coefficients, where low values will cause the objects to slow at a faster rate.

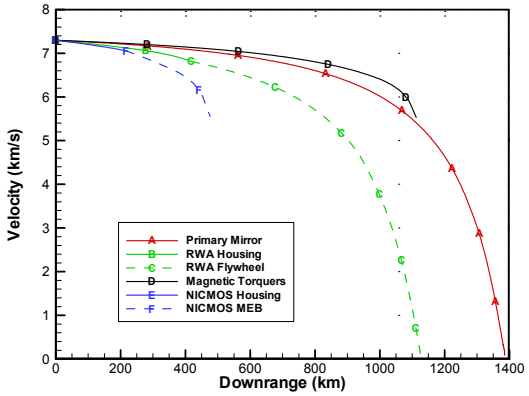

Figure 4. Velocity vs. downrange for sample objects.

4.2. Aerothermal

Fig. 5 shows the net heating rates as a function of time for the demising and surviving objects. The net heating rate will remain positive as long as the hot-wall heating rate plus the oxidation heating rate is greater than the surface re-radiation heating rate. A few of the objects will have a rising heating rate despite the decreasing velocity. This is due to the exponential change in atmospheric density as the object drops in altitude. The surviving objects have heating rates that initially increase but then drop rapidly to rates below zero. The objects continue to cool but tend to converge to a heating rate near zero for the last part of the trajectory.

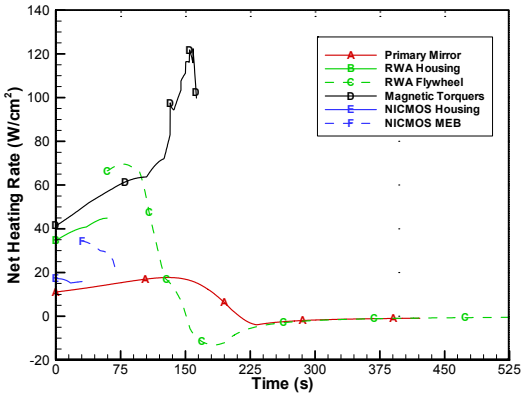

Figure 5. Net heating rate vs. time for sample objects.

In Fig. 6 the total absorbed heat of the objects are non-dimensionalized by the corresponding heat of ablation and plotted against time. When the value of absorbed heat divided by heat of ablation reaches 1.0, then the object is assumed to demise. All the demising objects reach the value of 1.0 and then stop because they have demised. The parent objects reach a value of 1.0, at which point it demises, and their fragment is exposed to aeroheating. The surviving objects reach a peak below 1.0 and then begin to shed heat, indicating that they did not burn up and will impact the ground.

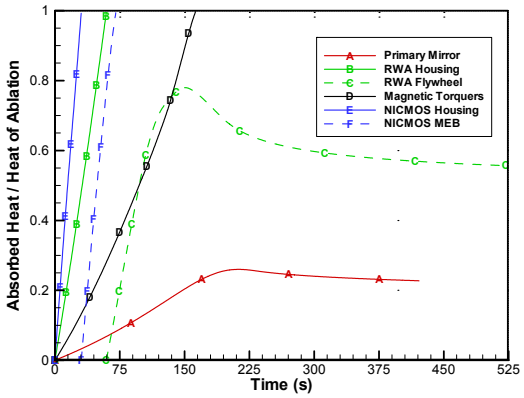

Figure 6. Ratio of absorbed heat to total heat of ablation for sample HST objects.

The surface temperatures of the sample objects are shown in Fig. 7. The demising objects are shown to reach their material melt temperature and then remain there until the entire object has ablated to the point of demise. The Magnetic Torquer consists of two material layers. It reaches the melt temperature (1700 K) of the first material (CRES). Then once that layer ablates, the temperature rises to the second material (Iron) layer melt temperature (1812 K). The Primary Mirror never reaches its high melt temperature (1760 K) before it begins to cool and impacts the ground. The RWA aluminum housing reaches its melt temperature of 867 K, and soon demises, exposing the RWA Flywheel. The RWA Flywheel reaches its melt temperature (1700 K) and loses a few layers of material but not enough to fully demise. It then begins to cool, and the surface temperature is seen to drop as the object approaches the earth.

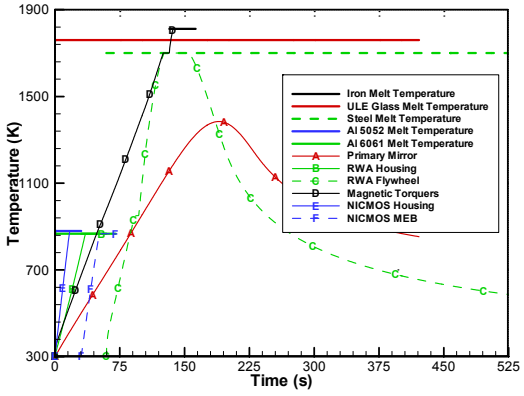

Figure 7. Surface temperature of sample objects.

4.3. Risk

Fig. 8 portrays the results after the breakup at 78 km. This figure plots the demise altitude of every object modeled. The objects that signify the heel and toe of the 1220 km survival footprint have been marked on the figure.

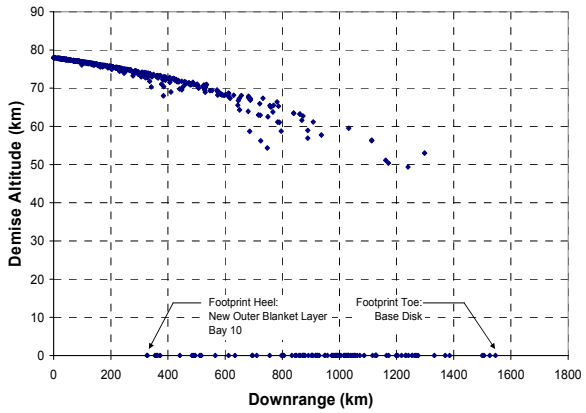

Figure 8. Demise altitude vs. downrange for all modeled HST components.

The analysis shows that 98 different components (some with multiple quantities) will survive. The total debris casualty area of the HST satellite orbital decay reentry was determined to be 156.1 m^2. However, a few of these surviving objects impact the ground at such a low velocity that they pose a very small risk of injury. Therefore, any items that impact below a 15-J threshold were ignored for the purposes of calculating risk. The remaining items total a debris casualty area of 146.2 m^2. The predicted impacting mass for all objects is 2055 kg, approximately 17.4% of the total estimated spacecraft mass.

Based upon the latest configuration and orbit of HST and on solar activity, HST is expected to reentry about 2021. The actual reentry year will be highly dependent upon the nature (absolute magnitude and duration) of the next solar maximum, currently expected about 2012.

Fig. 9 displays the risk of an HST reentry for the years ranging from 2011 to 2025. The risk is shown to increase each year due to a predicted increase in population. This risk ranges from 1:375 in the year 2011 to 1:325 in the year 2025. With the inclination angle of 28.5º and the expected reentry date of 2021, the resulting risk to population is 1:340. Since only 75% of the mass was analyzed, there remains a possible risk posed by the remaining 25%. If the risk from the remaining mass is scaled based on the risk of the analyzed mass, then the resulting weighted risk posed to the human population in the year 2021 is 1:250.

5. SUMMARY

This paper presented the results of a reentry survivability analysis of the Hubble Space Telescope performed with the ORSAT code. An orbital decay trajectory of the spacecraft parent body was considered from entry interface at 122 km down to assumed breakup at 78 km. Over 600 separate components of the HST were evaluated during entry, representing approximately 75% of the total mass of the spacecraft, with another 16% accounted for. Detailed plots of trajectory and aerothermal parameters were included in the debris assessment. The reentry of HST is predicted to produce a surviving mass of 2055 kg, and a total debris casualty area of 156.1 m^2. When ignoring the casualty area produced by objects under a 15-J threshold limit, the total debris casualty area becomes 146.2 m^2. For an orbital decay reentry in the year 2021 with a 28.5º inclination, this represents a casualty risk of 1:340. When the risk is adjusted based on the amount of unmodeled mass then the resulting weighted risk is 1:250. This risk is significantly higher than the acceptable value of 1:10,000 established by NASA Safety Standard 1740.14 (Gregory, 1995).

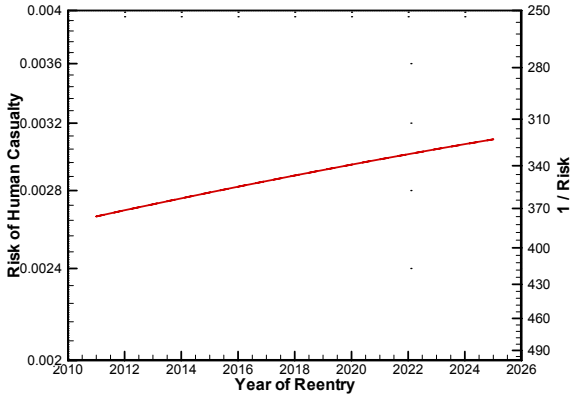

Figure 9. Risk calculation as a function of reentry year.

Due to the results of this analysis a decision has been made by NASA to perform a robotic mission to deorbit the spacecraft. Part of the mission will be to attach a de-orbit module to the satellite containing a propulsion system that will enable it to do a targeted reentry at the end of the science mission life.

6. REFERENCES

Cole, J. K. and Wolfe, W. P., Hazards to People and Aircraft from Flight Test Debris Generated at High Altitudes, AIAA-96-0070, 1996.

Detra, R. W., Kemp, N. H., and Riddell, F. R., Addendum to Heat Transfer to Satellite Vehicles Reentering the Atmosphere, *Jet Propulsion*, Vol. 27, No. 12, 1256-1257, 1957.

Dobarco-Otero, J., Marichalar, J. J., Smith, R. N., Opiela, J. N., and Rochelle, W. C., *Upgrades to Object Reentry Survival Analysis Tool (ORSAT),* JSC-29836, 2002. (Also Paper IAC-03-IAA.5.3.04 presented at 54th International Astronautical Congress, Bremen, Germany, September 29 – October 3, 2003).

Erickson, C.D. Reentry flight demonstration number one (RFE-1): design, development, and

performance of the reentry vehicle, Sandia Corporation SC-RR-64-511.

Fay, J. A. and Riddell, F. R., Theory of Stagnation Point Heat Transfer in Dissociated Air, *Journal of the Aeronautical Sciences*, Vol. 25, No. 2, 73-85, 1958.

Fritsche, B., Koppenwallner, G., Ivanov, M., et al. Advanced model for spacecraft disintegration during atmospheric reentry, ESOC Contract No. 12804/98/D/IM, Apr 2000.

Gregory, F. D., *NASA Safety Standard – Guidelines and Assessment Procedures for Limiting Orbital Debris*, NASA NSS 1740.14, Aug 1995.

Kerrod, Robin, *Hubble: the Mirror on the Universe*, Firefly Books (U.S.) Inc., Buffalo, NY, 2003.

Refling, O., Stern, R., and Potz, C., Review of Orbital Reentry Risk Predictions, Aerospace Corp. Report No. ATR-92(2835)-1, Jul 15, 1992.

Rochelle, W. C., Kirk, B. S., and Ting, B. C., *User's Guide for Object Reentry Survival Analysis Tool (ORSAT) – Version 5.0, Vols. I and II*, JSC-28742, 1999a.

Rochelle, W. et al. Modeling of space debris reentry survivability and comparison of analytical methods, paper IAA-99-IAA.6.7.03, *Proceedings of 50th IAC*, Amsterdam, the Netherlands, 1999b.

Rochelle, W.C. et al. Results of IADC reentry survivability benchmark cases: comparison of NASA ORSAT 5.0 code with ESA SCARAB code, *Proceedings of 17th IADC Meeting*, Darmstadt, Germany, 1999c.

Smith, R.N., Bledsoe, K.J., Dobarco-Otero, J., *Reentry Survivability Analysis of the Hubble Space Telescope (HST)*, JSC-62599, 2004.

Space Telescope Science Institute (STScI), HubbleSite, http://hubble.stsci.edu/sci.d.tech/, accessed Apr 2004.